RESEARCH ARTICLE

Loading of Artesunate with MIL100(Fe) Nanoparticles and Evaluation of Anti-cancer Activity in a Human Breast Cancer Cell Line

Murder AL Haydar[1]*, Ahmed Gedawy[2], Hussein R. Abide[3], Masoumeh Zargar[4], Naomi Brook[1], Crispin Dass[1], Bruce Sunderland[1]

[1]*Curtin Medical School, Faculty of Health Sciences, Curtin University, Bentley Western Australia, Australia*
[2]*Biotechnology and Drug Development Research Laboratory, Curtin Medical School, Curtin University, Bentley 6102, Australia*
[3]*Department of Chemical Engineering, Curtin University, GPO Box U1987, Perth, WA, 6845 Australia*
[4]*School of Engineering, Edith Cowan University, 270 Joondalup Drive, Joondalup, WA 6027 Australia*

Received: 02nd January, 2022; Revised: 08th February, 2022; Accepted: 05th March 2022; Available Online: 25th March, 2022

ABSTRACT

Artesunate (ART), an anti-malarial drug, is nowadays used for the treatment of several types of cancers. It is sparingly soluble in water; therefore, it requires the development of a modified formulation of this drug to enhance its water solubility and stability. MIL100(Fe) nanoparticles, a metal-organic framework, were selected as the drug carrier.

Purpose: This study aimed to employ MIL-100 (Fe) as a carrier for ART to investigate the release profile of ART and evaluate *in vitro* its anti-cancer activity.

Methods: ART loading was achieved by mixing ART with MIL100(Fe) in the proportion of (1:1) and (1:2) to form ART-1MIL100(Fe) and ART-2MIL100(Fe), respectively. Only ART-2MIL100(Fe) was coated with 0.5% chitosan (CH) to form CH-ART-2MIL100(Fe). Free ART, ART-2MIL100(Fe), and CH-ART-2MIL100(Fe) were evaluated for anti-cancer activity in a human breast cancer cell line.

Results: The ART loading capacity was 65% ± 1.3 and 75% ± 2.2 for ART-MIL100(Fe) and ART-2MIL100(Fe), respectively. The release profiles showed 50% ± 2.3 and 63% ± 1.5 of cumulative ART percent release for ART-2MIL100(Fe) and CH-ART-2MIL100(Fe), respectively. Although free ART demonstrated inhibition of cell viability (81%), ART-2MIL100(Fe) and CH-ART-2MIL100(Fe) showed cell inhibition viability of 56 and 51%, respectively.

Conclusion: ART loading within MIL100(Fe) was effective and *in vitro* breast anti-cancer effect was significant.

Keywords: Artesunate, Breast cancer, Chitosan, Drug release. MIL100(Fe).

International Journal of Drug Delivery Technology (2022); DOI: 10.25258/ijddt.12.1.72

How to cite this article: AL Haydar M, Gedawy A, Abide HR, Zargar M, Brook N, Dass C, Sunderland B. Loading of Artesunate with MIL100(Fe) Nanoparticles and Evaluation of Anti-cancer Activity in a Human Breast Cancer Cell Line. International Journal of Drug Delivery Technology. 2022;12(1):401-407.

Source of support: Nil.

Conflict of interest: None

INTRODUCTION

The development of nanoscale particle formulations as drug delivery systems to enhance drug efficacy and reduce drug side effects is well recognized.[1] Porous hybrid metal-organic frameworks (MOF) have received remarkable attention in recent decades.[2-5] The tailorable compositions, structures, excellent porosity, and tunable surface modification of MOF are among the porous material as drug carriers.[6] The drug loading capacity and efficient drug release profiles of MOF are the main challenges of using MOF nanoparticles (NPs) formulations.[7] Drug molecules are often simultaneously loaded into the MOFs either during synthesis or post-synthesis process.[8] MIL-100 (Fe) NPs are a popular MOF in biological applications since they are non-toxic and have relatively low catalytic activity in a physiological environment (pH 6.5–7.4).[9,10]

Artesunate (ART) has been known to be an anti-malarial drug for decades. However, its activity as a potent antiproliferative drug has also more recently been reported.[11,12] It is sparingly soluble in water, together with low aqueous stability, due to two methyl groups in its structure, as shown

**Author for Correspondence: muder.alhaydar@curtin.edu.au*

in Figure 1. Therefore, the activity and solubility of ART in biological media is pH dependent[13]. Consequently, using productive nanoparticle techniques for suitable drug delivery and release becomes crucial, especially within tumor tissue. ART has been reported as having anti-cancer activity in numerous tumors, including myelodysplastic syndrome,[14] chronic myeloid leukemia,[15] bladder cancer,[16] breast cancer,[17] and prostate cancer.[18]

Enhancing ART solubility by fabricating different nanoscale formulations has been reported by several researchers to increase its efficacy and provide a sustained release profile. The formulation and development of ART nanoparticles have usually employed polymers such as poly (lactic-co-glycolic acid) which were developed with chitosan by the emulsification-solvent evaporation technique and surface modification via physisorption methods.[19] ART loading into the lipid core of a polymer-lipid hybrid carrier increased both the anti-cancer activity and physical stability of ART.[20]

Chitosan is well known for developing conventional and novel drug delivery systems due to its different physicochemical properties, such as mucoadhesion and protonation. It promotes formulated nanoparticles to adhere to tumor cell membranes,[21] and several reports have shown that CH exerts a cytotoxic effect on different cancer cells [22] so was employed in this study. The aim of this study was to employ nanoparticles of MIL-100(Fe) as a carrier for ART before and after coating with CH and to evaluate their release profile and *in vitro* anti-cancer activity.

MATERIALS AND METHODS

Artesunate ($C_{19}H_{28}O_8$) was supplied by Apin Chemical Ltd, UK, trimesic acid (H_3BTC, $C_9H_6O_6$, 98%), acetic acid ($C_2H_4O_2$ 100%), dimethylformamide (DMF, 98%), ethanol (C_2H_6O, >95%) and chitosan (deacetylated chitin, Poly(D-glucosamine,) were purchased from Sigma Aldrich, Sydney, NSW, Australia. HPLC solvents, acetonitrile (C_2H_3N 99.9%), and phosphoric acid (H_3PO_4 85%) were sourced from Fisher Chemical, Belgium. The human breast cancer cell line (MDA-MB231) was purchased from the American Tissue Culture Collection (ATCC, USA).

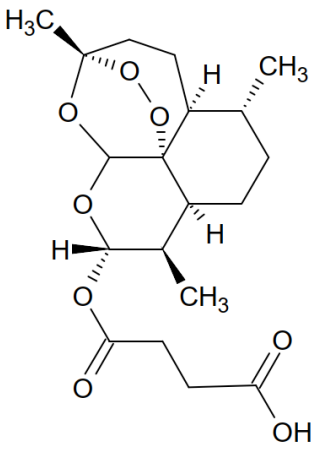

Figure 1: Chemical structure of Artesunate (ART).

Preparation of Fe-MIL100 NPs

MIL100 (Fe) NPs were prepared as previously described[23,24] by mixing 5 mmol of $FeCl_3 \cdot 6H_2O$ with 2.5 mmol of H_3BTC in 36 mL of distilled water in an autoclave of 125 mL capacity and heated in an oven at 160°C for 15 hours. The suspension was centrifuged, and the solid product was washed successively in water (350 mL, 70°C, and 3 hours) and then in ethanol (250 mL, 65°C, and 3 hours). The product was an orange-brownish powder and was dried at 90°C overnight.

Loading of ART with Fe-MIL100 NPs

ART was assayed by HPLC (Shimadzu 20 AC), and the mobile phase was 50 mmol phosphate buffer solution at pH 7 with 35% acetonitrile. Pre-dried 20 and 40 mg samples of MIL-100 (Fe) NP placed in two vials were separately mixed with a 20 mg ART in 20 mL of ethanol. The two vials were mixed for 24 hours at room temperature and then the mixtures were centrifuged (15000 rpm, 30 min). The supernatant was separated from the solid material and assayed by HPLC for the concentration of non-loaded ART. The solid material in the bottom of the test tubes represented ART-1MIL100 (Fe) and ART-2 MIL100 (Fe), respectively. These solid materials were washed with 5 mL of ethanol to remove any precipitated ART, dried at 60ºC for 30 minutes, and left overnight at room temperature. The loading percentage was calculated by subtracting the amount of ART in the supernatant from the amount of the ART before mixing and by employing the following Equation 1.

$$ART\ Loading\ \% = \frac{wt\ of\ ART\ in\ supernatant}{wt\ of\ ART\ before\ mixing}\ x\ 100 \quad ...(1)$$

Coating the ART-MIL100 (Fe) NPs with Chitosan

A solution of 0.5% CH in distilled water in 10 mL of 0.1% glacial acetic acid was prepared. An amount of 30 mg of solid material of ART-2MIL100 (Fe) NP was selected for CH coating and stirred with 10 mL of absolute ethanol for 30 minutes and then mixed with 10 mL of CH solution. The mixtures were centrifuged (15000 rpm, 30 minutes) and the produced solid materials were separated and dried at 60ºC for 1 hour. The products after drying were labeled CH-ART-2MIL100(Fe).

Characterization of Loaded and Coated MIL-100 (Fe) NPs

Powder X-ray diffraction measurements of MIL100 (Fe) NPs before and after ART loading and CH coating were used to examine the stability of MIL-100 (Fe) structure and confirm ART loading. The XRD was performed using a D8 Advance (Bruker AXS, Karlsruhe, Germany) with a Lynx Eye detector, a copper Kα radiation source (40 kV and 40 mA). The 2-theta scan range was 5°–30°. FTIR spectra were obtained to confirm chemical stability of MIL100 (Fe), ART loading, and CH coating; a PerkinElmer FTIR spectrometer was used at a wavenumber from 650 to 4,000 cm^{-1}. The morphological examination used a Zeiss Neon 40 EsB field-emission scanning electron microscopy (SEM) with SmartSEM software for MIL100(Fe) before and after ART loading and CH coating. Zeta potential was performed by using a Zeta sizer Nano-ZS (Malvern Instruments, Malvern, UK) at 298 K, and prior to measuring the Zeta potential, MIL100(Fe) samples

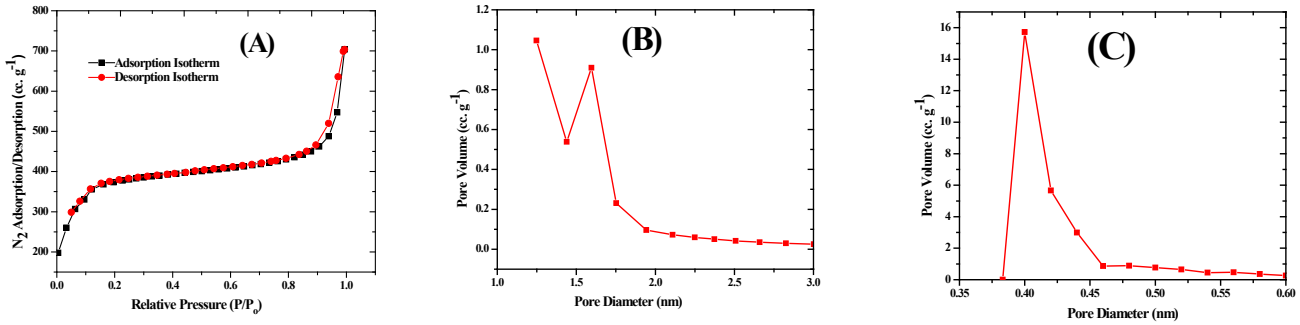

Figure 2: (A) N2 adsorption-desorption isotherms, (B) Mesopore distribution, and (C) Micropore distribution.

were dispersed in ethanol and stirred for 60 min at constant temperature (298 K).

ART Release Profile

The release profile of ART *in vitro* was carried out in phosphate buffer (PBS) solution at pH 7.4 by using a dissolution tester (Erweka DT6 unit). Predetermined quantitatively weighed samples of ART-2 MIL100 (Fe) and CH-ART-2 MIL100 (Fe) were submerged into 50 mL of dissolution medium (50 mmol PBS) at 37°C ± 1°C with a constant stirring at 100 pm. At predetermined time intervals, an aliquot of 0.5 mL was withdrawn and replaced with the same volume of fresh PBS. The aliquots were diluted and filtered by 0.2 µm syringe filter and analyzed using HPLC.

CellTiter Blue Assay

Cell viability was evaluated using the CellTiter-Blue assay. Exponentially growing MDA-MB231 breast cancer cell lines (90% confluent) were seeded onto 96 well plates at 1,000 cells/well in quadruplicate. Dulbecco's Modified Eagle's Medium-high glucose (DMEM) (Sigma), which included 10% fetal calf serum (FCS) and 1% antimycotic/antibiotic was used for cell propagation. After 24 hours, cells were treated with DMEM (negative control), doxorubicin (positive control, clinically used anti-cancer drug) at 5 µM final concentration, and 100 mM free ART. An equivalent amount of ART-2 MIL100 (Fe) and CH-ART-2 MIL100 (Fe) NPs were suspended in DMEM to deliver 100 µM final concentration of ART. The plates, including all treatments, were incubated for 48 hours before the addition of CellTiter-Blue Reagent (Promega) to test cell viability. Viable cell counts in all plates were determined from the microphotographs taken by Nikon Eclipse TS 100 light microscope (Nikon Eclipse TS 100 light microscope) for cell line imaging at (200X) magnification.

RESULTS

The N_2 adsorption-desorption isotherm for MIL100 (Fe) NP is shown in Figure 2. Figure 2a shows that N_2 adsorption was sharply increased when the relative pressure (p/p_o) was initially increased up to 0.0048. Then plateau region is demonstrated when the relative pressure is increased up to 0.9. In addition, both isotherms of adsorption and desorption are overlapped, showing a typical Type II BET isotherm. These

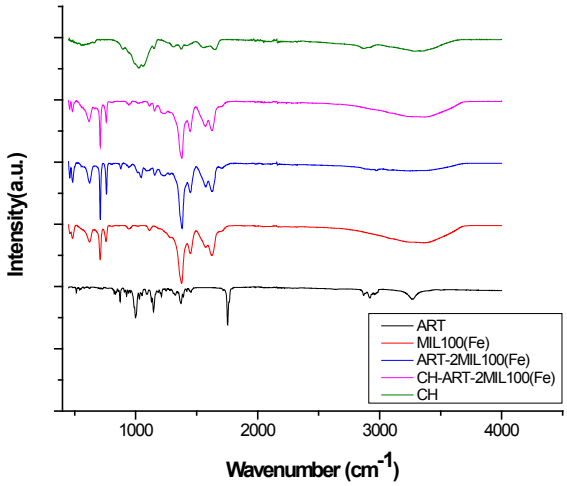

Figure 3: FTIR profiles of ART, MIL-100 (Fe), ART1@2MIL-100 (Fe), and CH@ART1@2 MIL-100 (Fe) and CH.

phenomena confirm that MIL100 (Fe) NPs are a microporous material. Figure 2b and c show the mesopore and micropore distributions, respectively. The pore distributions indicated the pore size was lower than 2 nm, the maximum pore size was approximately 1.6 nm, and the minimum pore size was 0.4 nm. BET surface area was 1487 $m^2.g^{-1}$, the micropore BET was 1301 $m^2.g^{-1}$, and the external surface area was 185.6 $m^2.g^{-1}$.

Loading percentages of ART-1MIL100 (Fe) and ART-2MIL100 (Fe) were 64 ± 1% and 75 ± 2% respectively. These results indicated that the loading capacity of NPs was increased when the amount of the NP was doubled, while further investigation showed that for higher amounts of NP, there was no increase in the loading capacity.

FT-IR spectra of ART, MIL100(Fe), loaded ART with NP, and coated product (Figure 3) were performed to investigate the possible interactions between the ART and MIL100 (Fe). Figure 3 shows the IR spectra of ART peak characteristics of O–H bending vibration at 3270 cm^{-1} and a band with a main strong peak at 1750 cm^{-1} indicative of the C=O stretch of the ester group.[25,26] The C–H in-plane vibration was displayed between 1212 and 980 cm^{-1}, and weak peaks of C–C stretching within the ring structures at 1456 cm^{-1} also showed some

stretching on ART-2 MIL100 (Fe) and CH-ART-2 MIL100 (Fe) spectra. The C–O vibration weak band at 1372 cm^{-1} of ART-2 MIL100 (Fe) and CH-ART-2 MIL100 (Fe) and other weak bands at 835 and 873 cm^{-1} were assigned to the CH_2 rocking vibrations.[27] CH_3 group at the band ranged from 980 to 835 cm^{-1} is obviously seen in the spectrum of ART-2 MIL100 (Fe), which indicates ART was loaded in MIL100 (Fe).

XRD patterns of ART, MIL100 (Fe), ART-2MIL100 (Fe) and CH-ART-2MIL100 (Fe) are shown in Figure 4. The peaks in XRD patterns of loaded and coated MIL-100 (Fe) were matched with those of MIL100 (Fe), which indicated the integrity of the structures was maintained as the structure of MIL100 (Fe) particles. The intensities of the peaks in the patterns of ART-2 MIL100 (Fe) and of CH-ART-2 MIL100 (Fe) were significantly reduced, while the peak positions in the XRPD patterns were similar.

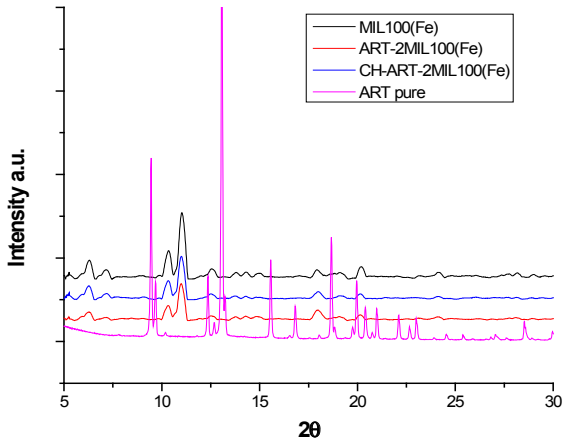

Figure 4: XRD of pure ART, MIL100 (Fe), ART-2 MIL100 (Fe), and CH-ART-2 MIL100 (Fe).

Figure 5 represents SEM images of A and a MIL100 (Fe), (B and b) ART-2 MIL100 (Fe), and (C and c) CH-ART-2MIL100 (Fe). The images show a monodisperse pyramid shape and rather uniform sizes of around 200 nm (a, b, and c). The thickness of the outer shell of ART-2MIL100 (Fe) and CH-ART-2MIL100 (Fe) indicate ART loading and CH coating. The CHART-2MIL-100 (Fe) image demonstrates crystals with rough surfaces due to the coating with CH.

The zeta potential measurements were obtained to confirm NPs stability and ART loading. The zeta potential was -2.1 ±0.4, 27.3 ±2.1 and 42 ±3 of MIL100 (Fe), ART-2MIL100 (Fe) and CH-ART-2MIL100 (Fe), respectively. Zeta potential measurements were positively increased in comparison to the bare MIL100 (Fe).

In vitro ART release profiles (Figure 6) show the cumulative release curves of ART from MIL-100(Fe) NP. After 36 h, about 50% ± 2.3 and 63% ± 1.5 of cumulative ART in ART-2 MIL100(Fe) and CH-ART-2MIL-100 (Fe) NPs respectively were released. Both profiles performed two periods of drug release; it commenced with rapid drug release followed by a plateau period of a constant rate of release. The release profile of CH-ART-2 MIL100 (Fe) was similar to ART-2 MIL100 (Fe), except the second period of profile showed a slow-release profile for 36 h and higher ART cumulative percent.

The *in vitro* anti-cancer activity of ART NPs was tested in breast cancer MDA-MB231cells which were treated with the various samples of the free ART, ART NPs, DMEM (negative control), and doxorubicin (positive control, anti-cancer drug) as shown in Figure 7. The results were statistically significant (p<0.05) for all ART samples, and these results indicated that ART inhibited the proliferation of MDA-MB231 cells.

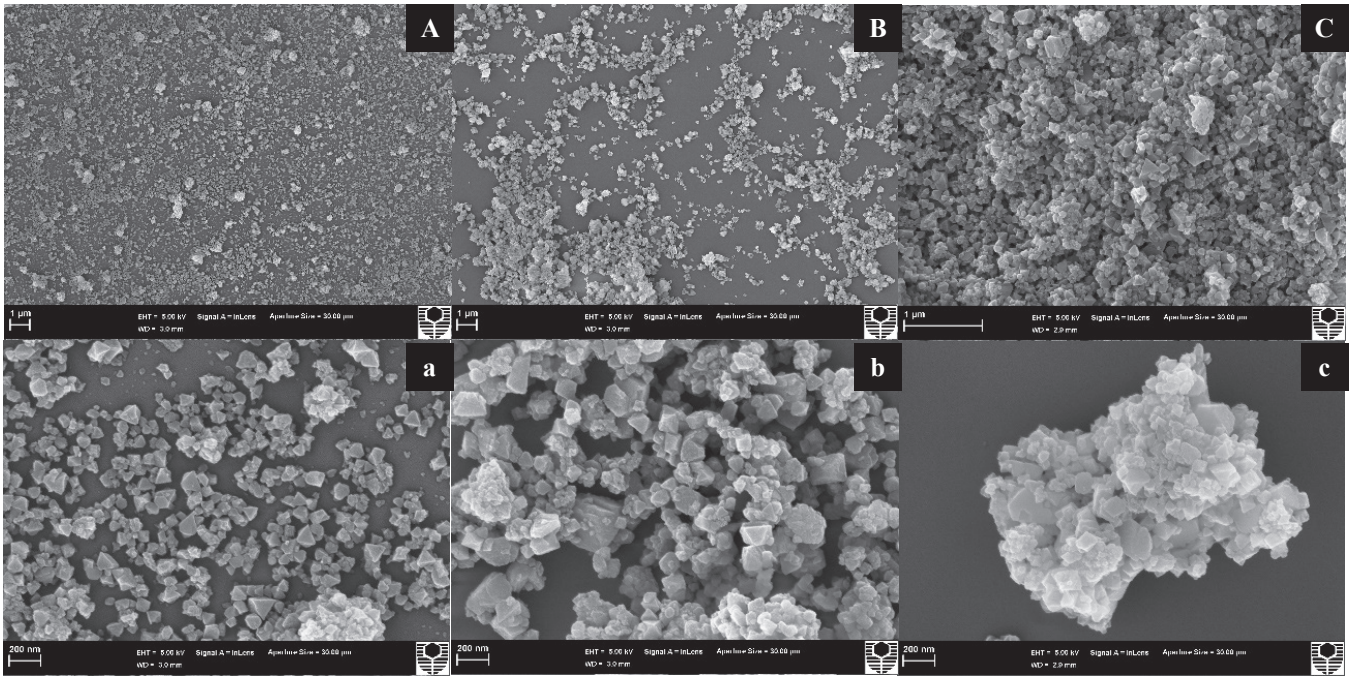

Figure 5: SEM images of (A and a) MIL-100 (Fe), (B and b) ART-2MIL100 (Fe), and (C and c) CH-ART-2MIL100 (Fe).

The NP2 (CH-ART-2MIL-100 (Fe)) has the most powerful anti-cancer effect compared to the doxorubicin and control. The free ART induced cell growth inhibition, but the cell viability was approximately 81%, while the cell viability with NP1 and NP2 were 56% and 51%, respectively, as shown in Figure 8.

DISCUSSION

The N_2 adsorption-desorption isotherm for MIL100 (Fe) NP has demonstrated mesopore, and micropore distributions of MIL100 Fe indicated that NPs have effective pore size and surface area. Owing to mesoporous structure, large specific surface area, and pore size of the MIL100(Fe), which can be hypothetical as ideal carriers to encapsulate ART.[28] The loading capacity of NPs was increased when the amounts of NPs was doubled. These results are attributed to its large BET surface area, which provided many active sites for ART to be adsorbed in MIL100 (Fe). However, a smaller pore size might increase the dispersion interactions of ART molecules inside the pores, which might reduce the opportunity of the electrostatic – interaction events. Still, the presence of high external surface area can significantly enhance the adsorption of ART.[29,30] FT-IR spectra of MIL100(Fe), ART-2 MIL100(Fe), and CH-ART-2MIL-100 (Fe) structures were intact, and these results were effectively indicated ART loading. The C–O vibration weak band at 1372 cm^{-1} indicated stretching on IR spectra of ART-2MIL100 (Fe) and CH-ART-2MIL100 (Fe), and other weak bands at 835 and 873 cm^{-1} were assigned to the CH_2 rocking vibrations.[27] The peaks at 2871, 2922, and 2968 cm^{-1} are assigned to C-H stretching of the CH_3 group, while C=O stretching was displayed at 1359 cm^{-1}. An O-H bending was seen at 1456 cm^{-1}.[26] The zeta potential result indicated the loading of ART within MIL100 (Fe) and the interaction between bridging hydroxyl groups of MIL100 (Fe) with the hydroxyl group of ART to form an ester bond. Therefore, the negativity of MIL100 (Fe) was reduced. The high positive zeta potential of CH-ART1-2MIL100 (Fe) indicates the presence of CH in the coating of ART.[31]

In vitro, ART release profiles demonstrated two periods of release. The first period of ART-2MIL100 (Fe) NPs release was 8 hours, and this was related to the high affinity of ART to diffuse through phosphate buffer solution at pH 7.4 rather than to be adsorbed on the surface of MIL100 (Fe) NPs. The second period of profile demonstrated demolishing of MIL100 (Fe) NPs because all MOFs cannot be stable in the alkaline

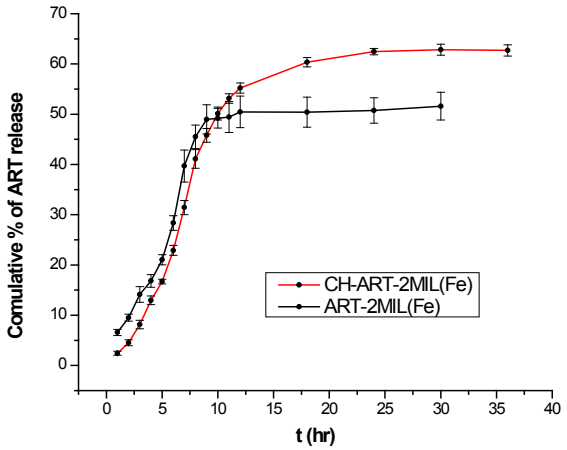

Figure 6: Artesunate (ART) release profiles in 50 mmol phosphate buffer solution at pH 7.4 and 37 °C.

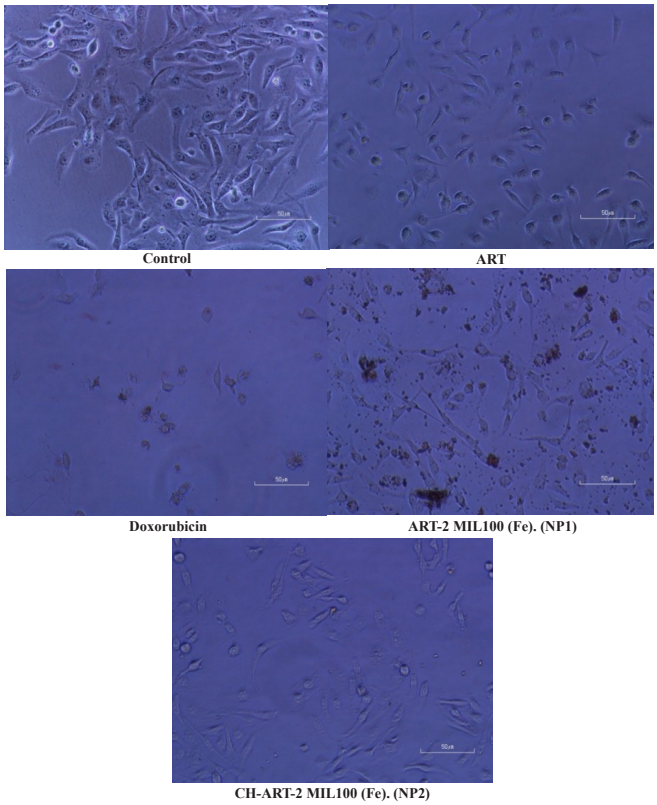

Figure 7: Microscopic images of viable cells of human breast cancer cells with control, ART, doxorubicin, NP1 (ART-2 MIL100 (Fe), NP2 (CH-ART-2MIL100 (Fe).

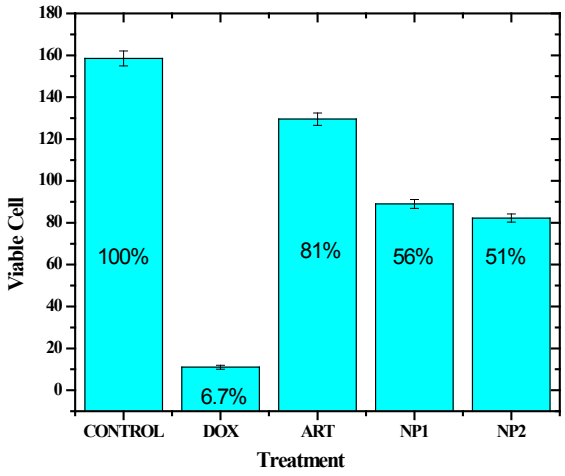

Figure 8: Microscopic counts of viable cells of human breast cancer cells with control, ART, doxorubicin, NP1 (ART-2 MIL100 (Fe), NP2 (CH-ART-2 MIL100 (Fe).

medium for longer than 24 hours.[32] The release profile of CH-ART-2MIL100 (Fe) was similar to ART-2MIL100 (Fe), except the second period was taking more extended time and that is related to the CH coating, which could be attributed to the ionic interaction of ART and CS coating layer.[33]

The *in vitro* anti-cancer activity of ART was tested in breast cancer demonstrated a significant effect and this suggest that the CH coating may allow CH-ART-2MIL100(Fe) (NP2) to specifically target cancer cells (MDA-MB-231) by the possibility of enhanced adhesion of CH-ART-2MIL100(Fe) to the cellular surface by CH and improved intracellular uptake.[10,20] Chitosan has anti-cancer activity itself.[22,34] Therefore, there could be a double benefit of using CH that increased adhesion of NP2 to the cancer cells and the direct anti-cancer activity of CH itself, which would complement ART. The difference in the percentage of cell growth inhibition between ART-2MIL100(Fe) and CH-ART-2MIL100(Fe) NPS correlates with the small difference between their release profiles of them. In addition to that, the MOF NPs themselves have anti-cancer activity as some studies later open a new approach about the potential anti-cancer effect of MOF NPs and the ability to target tumor tissue passively[10,35] The cytotoxicity of nanoparticles of ZIF-8 and its effect as anti-cancer with DOX@ZIF-8 showed high cytotoxicity to HepG-2 and MCF-7 cells compared with free DOX. These findings indicate that ZIF-8 nanoparticles are a promising anti-cancer cell.[36] Recently, nanoparticles of MOFs have been engineered for combined cancer therapy with synergistic efficacy and progressively promoted as a new class of theragnostic nanomedicine.[37]

CONCLUSIONS

MIL100(Fe) NPs are an appropriate carrier for ART as a drug delivery system. The loading capacity of MIL100(Fe) of ART increased but was not greater than 1:2. The loaded NPs were stable and had no drug interaction with NPs. The coating of NPs with CH has a significant effect on ART release profile and in the breast cancer cell growth inhibition.

ACKNOWLEDGMENTS

We acknowledge the Curtin Medical School, Faculty of Health Sciences and Engineering School, Curtin University for providing access to their laboratories and employing different instruments and materials. The authors acknowledge the use of Curtin University's microscopy and microanalysis facilities, whose instrumentation has been partially funded by the University, State, and Commonwealth Governments.

REFERENCES

1. Wilczewska AZ, Niemirowicz K, Markiewicz KH, Car H. Nanoparticles as drug delivery systems. Pharmacological reports. 2012;64(5):1020-1037.
2. Leaf-nosed bat. Encyclopædia Britannica Online; 2009.
3. Al Amery N, Abid HR, Al-Saadi S, Wang S, Liu S. Facile directions for synthesis, modification, and activation of MOFs. Materials Today Chemistry. 2020;17:100343. Available from: https://www.sciencedirect.com/science/article/pii/S2468519420301038
4. Rada Z, Abid H, Sun H, Wang S. Bifunctionalized metal-organic frameworks, UiO-66-NO_2-N (N=-NH_2,-$(OH)_2$,-$(COOH)_2$), for enhanced adsorption and selectivity of CO_2 and N_2. 2015
5. Azhar MR, Abid HR, Periasamy V, Sun H, Tade MO, Wang S. Adsorptive removal of antibiotic sulfonamide by UiO-66 and ZIF-67 for wastewater treatment. Journal of colloid and interface science. 2017;500:88-95.
6. Sun C-Y, Qin C, Wang X-L, Su Z-M. Metal-organic frameworks as potential drug delivery systems. Expert opinion on drug delivery. 2013;10(1):89-101.
7. Bag PP, Wang D, Chen Z, Cao R. Outstanding drug loading capacity by water-stable microporous MOF: a potential drug carrier. Chemical Communications. 2016;52(18):3669-3672.
8. Cai W, Chu CC, Liu G, Wáng YXJ. Metal-organic framework-based nanomedicine platforms for drug delivery and molecular imaging. Small. 2015;11(37):4806-4822.
9. Sun L, Xu Y, Gao Y, Huang X, Feng S, Chen J, *et al*. Synergistic Amplification of Oxidative Stress–Mediated Antitumor Activity via Liposomal Dichloroacetic Acid and MOF-Fe2+. Small. 2019;15(24):1901156.
10. Ji P, Wang L, Wang S, Zhang Y, Qi X, Tao J, *et al*. Hyaluronic acid-coated metal-organic frameworks benefit the ROS-mediated apoptosis and amplified anti-cancer activity of Artesunate. Journal of drug targeting. 2020;28(10):1096-1109.
11. Liu WM, Gravett AM, Dalgleish AG. The anti-malarial agent artesunate possesses anti-cancer properties that can be enhanced by combination strategies. International Journal of Cancer. 2011;128(6):1471-1480.
12. Ho HN, Do TT, Nguyen TC, Yong CS, Nguyen CN. Preparation, characterisation and *in vitro*/*in vivo* anti-cancer activity of lyophilised artesunate-loaded nanoparticles. Journal of Drug Delivery Science and Technology. 2020;58:101801.
13. Al Hayder M, Sunderland V. Effect of hydroxypropyl-ß-cyclodextrin complexation on the aqueous solubility and stability of Artesunate. Int J Pharm Pharm Sci. 2014;6(7):598-601.
14. Xu N, Zhou X, Wang S, Xu L-l, Zhou H-s, Liu X-l. Artesunate induces SKM-1 cells apoptosis by inhibiting hyperactive β-catenin signaling pathway. International journal of medical sciences. 2015;12(6):524.
15. Kim C, Lee JH, Kim S-H, Sethi G, Ahn KS. Artesunate suppresses tumor growth and induces apoptosis through the modulation of multiple oncogenic cascades in a chronic myeloid leukemia xenograft mouse model. Oncotarget. 2015;6(6):4020.
16. Zuo W, Wang Z-Z, Xue J. Artesunate induces apoptosis of bladder cancer cells by miR-16 regulation of COX-2 expression. International journal of molecular sciences. 2014;15(8):14298-14312.
17. Chen K, Shou L-M, Lin F, Duan W-M, Wu M-Y, Xie X, *et al*. Artesunate induces G2/M cell cycle arrest through autophagy induction in breast cancer cells. Anti-cancer drugs. 2014;25(6):652-662.
18. Wang Z, Wang C, Wu Z, Xue J, Shen B, Zuo W, *et al*. Artesunate suppresses the growth of prostatic cancer cells through inhibiting androgen receptor. Biological and Pharmaceutical Bulletin. 2017;40(4):479-485.
19. Chen H-l, Wang Y-x, Zhou P, Liu R, Nan W-b, Wang Y-s, *et al*. Chitosan surface-modified PLGA nanoparticles: preparation, characterization, and evaluation of their *in vitro* drug-release behaviors and cytotoxicities. Current Nanoscience. 2014;10(2):255-262.

20. Tran TH, Nguyen TD, Poudel BK, Nguyen HT, Kim JO, Yong CS, *et al*. Development and evaluation of artesunate-loaded chitosan-coated lipid nanocapsule as a potential drug delivery system against breast cancer. Aaps Pharmscitech. 2015;16(6):1307-1316.
21. Prabaharan M. Chitosan-based nanoparticles for tumor-targeted drug delivery. International journal of biological macromolecules. 2015;72:1313-1322.
22. Alamry KA, Hussein MA, Al-Ghamdi YO, Saleh TS, Asiri AM, Alhebshi AM. Potential anti-cancer performance of chitosan-based β-ketosulfone derivatives. Cogent Chemistry. 2018;4(1):1559435.
23. Al Haydar M, Abid HR, Sunderland B, Wang S. Multimetal organic frameworks as drug carriers: aceclofenac as a drug candidate. Drug design, development and therapy. 2018;13:23-35. doi:10.2147/DDDT.S182983
24. Al Haydar M, Abid HR, Sunderland B, Wang S. Metal-organic frameworks as a drug delivery system for flurbiprofen. Drug design, development and therapy. 2017;11:2685-2695. doi:10.2147/DDDT.S145716
25. Rada ZH, Abid HR, Shang J, Sun H, He Y, Webley P, *et al*. Functionalized UiO-66 by Single and Binary (OH)2 and NO2 Groups for Uptake of CO2 and CH4. Industrial & Engineering Chemistry Research. 2016;55(29):7924-7932. doi:10.1021/acs.iecr.5b04061
26. Lawal A, Umar R, Abubakar M, Faruk U, Wali U. FTIR and UV-Visible spectrophotometric analyses of artemisinin and its derivatives. Journal of Pharmaceutical and Biomedical Sciences. 2012;24(24):6-14.
27. Setyawan D, Sari R, Yusuf H, Primaharinastiti R. Preparation and characterization of artesunate-nicotinamide cocrystal by solvent evaporation and slurry method. Asian J Pharm Clin Res. 2014;7(1):62-65.
28. Wang D, Zhou J, Chen R, Shi R, Xia G, Zhou S, *et al*. Magnetically guided delivery of DHA and Fe ions for enhanced cancer therapy based on pH-responsive degradation of DHA-loaded Fe3O4@C@MIL-100 (Fe) nanoparticles. Biomaterials. 2016;107:88-101.
29. Li J, Shen S, Kong F, Jiang T, Tang C, Yin C. Effects of pore size on *in vitro* and *in vivo* anti-cancer efficacies of mesoporous silica nanoparticles. RSC advances. 2018;8(43):24633-24640.
30. Zaboon S, Abid HR, Yao Z, Gubner R, Wang S, Barifcani A. Removal of monoethylene glycol from wastewater by using Zr-metal organic frameworks. Journal of colloid and interface science. 2018;523:75-85.
31. Guo C, Gemeinhart RA. Understanding the adsorption mechanism of chitosan onto poly (lactide-co-glycolide) particles. European journal of pharmaceutics and biopharmaceutics. 2008;70(2):597-604.
32. Li X, Lachmanski L, Safi S, Sene S, Serre C, Grenache J-M, *et al*. New insights into the degradation mechanism of metal-organic frameworks drug carriers. Scientific reports. 2017;7(1):1-11.
33. Ho HN, Tran TH, Tran TB, Yong CS, Nguyen CN. Optimization and characterization of artesunate-loaded chitosan-decorated poly (D, L-lactide-co-glycolide) acid nanoparticles. Journal of Nanomaterials. 2015;2015
34. Abedian Z, Moghadamnia AA, Zabihi E, Pourbagher R, Ghasemi M, Nouri HR, *et al*. Anticancer properties of chitosan against osteosarcoma, breast cancer and cervical cancer cell lines. Caspian Journal of internal medicine. 2019;10(4):439.
35. Cai M, Chen G, Qin L, Qu C, Dong X, Ni J, *et al*. Metal-organic frameworks as drug targeting delivery vehicles in the treatment of cancer. Pharmaceutics. 2020;12(3):232.
36. El-Bindary AA, Toson EA, Shoueir KR, Aljohani HA, Abo-Ser MM. Metal-organic frameworks as efficient materials for drug delivery: Synthesis, characterization, antioxidant, anti-cancer, antibacterial and molecular docking investigation. Applied Organometallic Chemistry. 2020;34(11):e5905.
37. Zhou J, Tian G, Zeng L, Song X, Bian Xw. Nanoscaled Metal-Organic Frameworks for Biosensing, Imaging, and Cancer Therapy. Advanced healthcare materials. 2018;7(10):1800022.